Published in final edited form as:
J Int Neuropsychol Soc. 2009 September ; 15(5): 671–683. doi:10.1017/S1355617709990233.

Molecular neurodevelopment: An *in vivo* ^{31}P-^{1}H MRSI study

Gerald Goldstein[1], **Kanagasabai Panchalingam**[2], **Richard J. McClure**[2], **Jeffrey A. Stanley**[6], **Vince D. Calhoun**[7,8], **Godfrey D. Pearlson**[9], and **Jay W. Pettegrew**[2,3,4,5]

[1]VA Pittsburgh Healthcare System, Pittsburgh, PA

[2]Department of Psychiatry, University of Pittsburgh School of Medicine, University of Pittsburgh, Pittsburgh, PA

[3]Department of Neurology, University of Pittsburgh School of Medicine, University of Pittsburgh, Pittsburgh, PA

[4]Department of Behavioral and Community Health Sciences, University of Pittsburgh School of Medicine, University of Pittsburgh, Pittsburgh, PA

[5]Department of Bioengineering, University of Pittsburgh, Pittsburgh, PA

[6]Psychiatry and Behavioral Neurosciences, Wayne State University School of Medicine, Detroit, MI

[7]The Mind Research Network, Albuquerque, NM

[8]Department of Electrical and Computer Engineering, University of New Mexico, Albuquerque, NM

[9]Department of Psychiatry, Yale University, Hartford, CT

Abstract

Synaptic development and elimination are normal neurodevelopmental processes which if altered could contribute to various neuropsychiatric disorders. ^{31}P-^{1}H magnetic resonance spectroscopic imaging and structural MRI exams were conducted on 106 healthy children ages 6–18 years in order to identify neuromolecular indices of synaptic development and elimination. Over the age range studied, age-related changes in high-energy phosphate (phosphocreatine), membrane phospholipid metabolism (precursors and breakdown products), and gray matter were found. These neuromolecular and structural indices of synaptic development and elimination are associated with development of several cognitive domains and changes in gray matter volume. Monitoring of these molecular markers is essential for devising treatment strategies for neurodevelopmental disorders.

Keywords

MRS; Neuroimaging; Metabolism; Cognition; Multiple Regression

INTRODUCTION

The four major stages that characterize human brain development are: 1) neuronal proliferation; 2) migration of neurons to specific sites throughout the CNS; 3) organization of the neuronal circuitry; and 4) myelination of the neuronal circuitry (Volpe, 1995).

Contact Address: Jay W. Pettegrew, M.D. Director, Neurophysics Laboratory, RIDC Park, 260 Kappa Drive, Pittsburgh, PA 15238. Phone: 412-967-6509 FAX 412-967-6563, pettegre+@pitt.edu .

There is no conflict of interest on the part of any of the authors.

The third stage of human brain development, organization of the neural circuitry, is most active from the sixth month of gestation to young adulthood. The major events associated with neuronal circuitry organization include: 1) proper alignment, orientation, and layering of cortical neurons; 2) dendritic and axonal differentiation; 3) synaptic development; 4) synaptic elimination (cell death and/or selective elimination of neuronal processes); and 5) glial proliferation and differentiation. These processes overlap with the timing of normal development of cognitive function and the onset of neurodevelopmental and psychiatric disorders such as attention deficit disorder, autism and schizophrenia. Normal synaptic elimination occurs during early adolescence in non-human primates (Rakic et al., 1986; Bourgeois & Rakic, 1993) and humans (Huttenlocher, 1979; Huttenlocher et al., 1982; Huttenlocher, 1990; Huttenlocher & Dabholkar, 1997). Synaptic elimination in non-human primates is generally observed to occur synchronously in all regions (i.e., homochronous) (Rakic et al., 1986) but is heterochronous in humans (Huttenlocher et al., 1997). Normal synaptic elimination is predominantly of presumptive excitatory asymmetric junctions on dendritic spines (Smiley & Goldman-Rakic, 1993) which probably utilize amino acids, such as L-glutamate, as the neurotransmitter (Storm-Mathisen & Otterson, 1990). Perinatal insults, intrauterine disturbances, and perhaps environmental influences in childhood and adolescence can potentially result in disordered neuronal circuitry (Birch & Gussow, 1970). This study focuses on molecular and structural indices related to synaptic development and elimination.

^{31}P and ^{1}H magnetic resonance spectroscopic imaging (^{31}P-^{1}H MRSI) are well suited to monitor the processes of synaptic development and elimination, and neuronal cell death by measuring energy dynamics [phosphocreatine (PCr)], a putative biomarker of neurons and neuronal processes [N-acetylaspartate (NAA)] and measures of membrane phospholipid metabolism, such as phospholipid building blocks [short NMR correlation time phosphomonoesters (sPME)] and phospholipid breakdown products [short NMR correlation time phosphodiesters (sPDE)]. The hypothesis tested in this study is that neuromolecular underpinnings of synaptic development and elimination will be observed by changes in ^{31}P-^{1}H MRSI observed brain metabolites of individuals ages 6–18, and will be associated with changes in percent of gray matter reflecting synaptic development and elimination. Specifically, we investigated in an axial brain slice cross-sectional age differences in brain levels of PCr, sPME, sPDE, and NAA which reflect changes in neuronal synaptic activity (PCr), neuronal numbers and integrity (NAA), turnover of membrane phospholipids (sPME and sPDE) and the percent gray matter. We hypothesized the above neurodevelopmental metabolic and structural changes would be associated with corresponding development of cognitive function in the domains of language, visual spatial constructional, executive function, and memory abilities. In an age difference study, one should expect to find meaningful correspondences among cognitive growth, the above brain metabolite levels, and percent gray matter.

METHODS

Participants

The study was approved by the University of Pittsburgh Institutional Review Board. All subjects (and parents when appropriate) gave informed written consent to participate in the study. Personal interviews including the subject and family were conducted by a psychologist and following the informed consent procedure and execution of the appropriate consent form, procedures were accomplished to assure that recruited participants were healthy, normally developing individuals who met all inclusion/exclusion criteria: These included a review of the study inclusion/exclusion criteria and completion and review of the Devereux Scale for Mental Disorders and a cognitive test battery as described below. This interview was followed by a separate interview where magnetic resonance (MR) exclusion criteria were reviewed by

an MR Center nurse or technician and by subject participation in an MR simulator. A pediatrician conducted the physical examination in an examination room at the MR Center. In addition to the report by the pediatrician, the Devereux, FH-DRC interview, and other tests from the cognitive neurodevelopmental battery were scored and reviewed with the subject and family. If all entry criteria were met, the full battery was completed followed by the entry time-point MRSI/MRI examination within one month after completion of the cognitive neurodevelopmental battery.

The sample consisted of 106 individuals ranging in age from 6 to 17. Fifty four were females and 51 were males. The age distribution covered the neurodevelopmental stages of childhood (6–10 years), pubescence (10–12 years), and adolescence (12–18 years). Many of these subjects also participated in the longitudinal component of the study involving evaluations on four occasions over a four year period. The longitudinal data will be reported separately. The present study only deals with data obtained at the first time point.

Neurocognitive Testing Procedures

A portion of the cognitive battery consisting of standardized tests with published manuals was administered using standard procedures under the supervision of a licensed psychologist in order to evaluate basic intellectual and academic abilities, and to detect behavioral abnormalities. This preliminary battery included an age appropriate version of the Wechsler intelligence scale [abbreviated WISC-R (1974) for children; WASI (1999) for adults] and the Wechsler Individual Achievement Test Screener (2001) to identify individuals functioning within the average range of intellectual ability (IQ 85-119) with commensurate progress in the acquisition of basic academic skills. Testing was typically completed in less than four hours. In addition to satisfying criteria for non-significant variance in intellectual ability, individuals demonstrating significant VIQ-PIQ score discrepancies (greater than 15 points) were eliminated from the study owing to the potential for possible asymmetric cognitive development. Any potential participant manifesting a significant discrepancy between IQ and reading and/or math development also was eliminated owing to the potential of confounds associated with an underlying learning disability. The Devereux Scale for Mental Disorders (1994) was used to assess social and emotional development. A T-score on any of the Devereux Scales (conduct, attention, anxiety, depression, autism, acute problems) ≥ 60 eliminated a child from the study owing to potential confounds associated with psychopathology. The FH-RDC (Andreasen et al., 1977) interview was given to rule out DSM-IV psychiatric disorders in first degree relatives. A pediatrician performed a medical examination, including Tanner staging of physical development, for each child at entry into the study as well as the 1, 2, and 3 year longitudinal follow-up to correspond with the MR examination. All tests included in the battery are appropriate for use across the age span of the study, are developmentally sensitive and have established age norms. The full neurocognitive battery included measures of cognitive domains divided here into language, visual spatial constructional, executive function, and memory abilities. The specific tests assigned to each domain are listed in Table 1. A composite score was computed for each domain by adding the scores of the tests and dividing by the number of tests used.

A set of test variables from the entire battery were selected to assess the cognitive domains of language, visual spatial, executive function, and memory. The cognitive domain scores were used for determination of associations with selected MRSI variables and percent gray matter. The first step was determining which of these cognitive measures, if any, were associated with the three MRSI variables, PCr, sPME/sPDE, and NAA. This analysis was followed by determining if synaptic elimination represented by percent gray matter was associated with the values of PCr, sPME/sPDE, and NAA. It was predicted that changes in one or more of the molecular indices obtained through the use of curve fitting procedures would coincide with or

precede evidence of synaptic development and elimination. Cognitive tests were used to evaluate the overall strength of association among cognitive function, the targeted metabolites, and gray matter volume.

MR Procedures

MRI and MRSI procedures were conducted using a doubly tuned transmit/receive volume head coil on a GE LX 1.5-T whole-body MRI system (GE Medical Systems, Milwaukee, Wisconsin). A three-dimensional volume of T1-weighted images covering the entire brain [spoiled gradient recalled acquisition (SPGR), repetition time (TR) = 25 ms, echo time (TE) = 5 ms, flip angle = 40°, field of view (FOV) = 240×180mm, slice thickness = 1.5mm, 124 coronal slices, number of excitations = 1, matrix = 256×192, and scan time = 7m 44 s] was then collected for tissue-segmentation analysis of the ^{31}P spectroscopy voxels. In addition a set of T2-weighted/proton density images (two-dimensional fast spin-echo; TR = 3000 ms; echo times = 17 and 102ms; echo-train length = 8; FOV = 240×240 mm^2; approximately 24 axial slices, 5-mm thick, and no gap; number of excitations = 1; matrix = 256×192; and scan time 5m 12 s) to screen for neuroradiological abnormalities.

^{31}P MRSI Acquisition—In order to prescribe the MRSI slice location, a 3-plane MRI localizer image was first collected, followed by a set of sagittal and axial scout images using the two-dimensional fast spin-echo sequence. Using the mid-sagittal image the anterior commissure-posterior commissure (AC-PC) line was defined and a 30 mm axial slice was positioned parallel to and superior to the AC-PC line for the spectroscopy (Figure 1A). Prior to the spectroscopy, automatic and manual shimming was applied to the axial slice. A single-slice selective excitation radio frequency (RF) pulse followed by phase-encoding pulses to spatially encode the two dimensions of the slice (termed FIDCSI on a GE system) was used to acquire the multi-voxel in vivo ^{31}P spectroscopy data. An example of quantified ^{31}P spectroscopy data, which is collected as described above, is shown in Figure 2. The acquisition parameters were FOV = 240×360 mm^2, slice thickness = 30 mm, 8×8 phase encoding steps (nominal voxel volume = 3.0×4.5×3.0 cm^3), TR = 2000 ms, complex data points = 1024, spectral bandwidth = 5.0 kHz, pre-acquisition delay = 1.7ms, number of averages = 16, and acquisition time approximately 34 minutes.

^{1}H MRSI Acquisition—This acquisition method combined the PRESS sequence (Bottomley, 1987) with the phase encoding steps of a chemical shift imaging (CSI) sequence, which is termed PRESSCSI and is part of the GE spectroscopy package. Briefly, the 90E RF pulse followed by two 180E RF pulses, which make-up this double-echo sequence, are all slice selective and the intersection of the three orthogonal planes defines a large region of interest (ROI). In this study the ROI is positioned in the axial plan and the left-right and anterior-posterior dimensions will vary accordingly to ensure the ROI covers the brain in the defined axial plane. Surrounding the ROI in the axial plan are four spatially localized saturation slices to suppress the strong lipid signal at the corners of the ROI. Very selective suppression pulses are used for the PRESS localization and the lipid saturation, which provide a much sharper excitation slice profile relative to conventional pulses (Roux, 1998). An example of quantified short TE ^{1}H spectroscopy data, which is collected as described above, is shown in Figure 3. The experimental parameters for the water suppressed PRESSCSI measurement were: FOV=240 mm, thickness of the ROI slice= 20 mm, phase encoding steps = 16×16 (nominal voxel dimension = 1.5×1.5×2 cm^3), TR = 1,500 ms, TE = 30 ms, complex data points = 2,048, spectral bandwidth = 2.5 kHz, and NEX = 2. Using identical experimental parameters, water unsuppressed PRESSCSI data were also collected for post-processing purposes, except there are 8×8 phase encoding steps.

MRSI post-processing and quantification—To minimize the partial volume effect for the sampled regions, six different voxel grid shift schemes (Figure 1A) were applied to both ^{1}H and ^{31}P MRSI prior to two-dimensional inverse Fourier transformation (2D IFT). These grid schemes provided voxels that include left and right: prefrontal cortex (LPFC, RPFC); superior temporal cortex (LSTC, RSTC); inferior parietal cortex (LIPC, RIPC); basal ganglia (LBG, RBG); and centrum semiovale (LCS, RCS).

Spectral fitting of ^{31}P MRSI—For ^{31}P MRSI, a mild spatial apodization was applied in k-space (Fermi window with 90% diameter and 5% transition width) resulting in an effective voxel size of approximately 46.4 cm^3, whereas a 5 Hz Gaussian apodization is applied in the chemical shift domain and PME, Pi, PDE, PCr, ∀-, ∃-, and (-ATP, and Pi were modeled in the time domain with Gaussian-damped sinusoids and by omitting the first 2.75 ms of the free induction decay (FID) using the Marquardt-Levenberg algorithm (Figure 2). This approach ensured that PME and PDE resonances primarily reflected freely mobile short NMR correlation time components (Stanley & Pettegrew, 2001). ^{31}P MRSI quantification was expressed in relative mole percent of the observable ^{31}P resonances. The mole percent method of quantification highly correlates with absolute quantification methods (Klunk et al., 1994). Reliability results (relative mole percent of observable phosphorus resonances ∀ *SD* and the CV in parentheses] for the multi-voxel obtained ^{31}P MRSI metabolites quantification are: sPME, 10.4 ∀ 2.0 (19%); Pi, 5.4 ∀ 1.3 (24%); sPDE, 28.5 ∀ 3.3 (12%); PCr, 11.3 ∀ 1.4 (13%); ∀ATP, 14.3 ∀ 2.0 (14%); ∃ATP, 16.3 ∀ 2.1 (13%); and ATP, 13.8 ∀ 2.6 (19%).

Spectral fitting of short TE ^{1}H MRSI—The residual of the unsuppressed water signal between 7 ppm and 4.2 ppm was removed by using the (operator-independent) SVD-based fitting algorithm (de Beer & van Ormondt, 1992). The LC Model software package was used to quantify the ^{1}H metabolites which include: NAA, glutamate, glutamine, myo-inositol, trimethylamines (TMA), total creatine (creatine + phosphocreatine; Cr_t), taurine, alanine, aspartate, GABA, glucose, scyllo-inositol, ɴ-acetylaspartylglutamate (NAAG), and the macromolecule signals. The key in simplifying the fitting of the complex overlapping resonances was to incorporate a priori knowledge into the fitting algorithm (deGraaf & Bovee, 1990; Provencher, 1993; Stanley et al., 1995). This included a priori knowledge of the macromolecule signals as part of the basis of LC Model (Seeger et al., 2003). The LC Model software package, which is commercially available, provided this feature and has been demonstrated by others (Brockmann et al., 1996; Frahm & Hanefeld, 1996; Ebert et al., 1997) to be an accurate and reliable method to quantify short TE ^{1}H MRS data. Our studies gave mean absolute levels, relative to the unsuppressed water signal and appropriate correction factors, and coefficient of variation (CV) of the prominent ^{1}H metabolites as: NAA, 7.41 mM (9.4%); Cr_t, 5.36 mM (13.5%); GPC + PC, 1.44 mM (16.8%); myo-inositol, 4.18 mM (20.8%); glutamate, 6.53 mM (20.4%); glutamine 2.77 mM (51.8%); and combined macromolecule signal 5.94 (33.4%) (scaled to H_2O resonance but uncorrected for relaxation times and total number of observable protons). Quantification of the NAA resonance was most reliable (CV = 9.4%); however, measures of glutamate and myo-inositol are more variable (CV = 20%) and glutamine is highly variable (CV = 52%). The mean absolute metabolite levels and the variance were consistent with prior short TE studies at 1.5T (Bartha et al., 2000; Brockmann et al., 1996; Ebert et al., 1997; Frahm et al., 1996; Kreis, 1997; Provencher, 1993; Stanley et al., 1995). These CV values demonstrate sufficient reliability enabling us to conduct short TE ^{1}H MRSI studies for the hypotheses to be tested. The post-processing was fully automated, required no operator input, and quantification results were 100% reproducible. An example of processed in vivo ^{1}H spectrum of a healthy individual using the proposed short TE ^{1}H MRSI technique and the postprocessing protocol is shown in Figure 3. Proton MRSI quantification was expressed as relative mole percent of observable proton resonances.

Morphometry—A fully automated segmentation procedure was used to segment T1-weighted 3D SPGR images. The functional magnetic resonance imaging of the brain (FMRIB) software Library (FSL) (Smith et al., 2004; Woolrich et al., 2009) (FSL Analysis Group, FMRIB, Oxford, UK) was used to co-register, correct for any B_1 field bias, brain extraction and segmentation. The axial slices from the 3D-SPGR images were co-registered to the axial scout images using FMRIB's linear image registration tool (FLIRT) of the FSL package. The brain extraction tool (BET) software was used to extract brain by removing non-brain matter from the image. The FMRIB's automated segmentation tool (FAST) was used to segment the brain into gray, white and CSF/extra cortical space while also correcting for spatial intensity variations (also known as bias field or B_1 field inhomogenity correction). Tools from the software package FreeSurfer (http://surfer.nmr.mgh.harward.edu) was used to convert the MRI images from ANALYZE format to neuroimaging informatics technology initiative (NIFTI) format, extract header information, and intensity normalization prior to segmentation.

The tissue fractions were then calculated by extracting from the segmented images the region of interest matching the coordinates and size of the ^{31}P spectroscopy voxels using miscellaneous FSL utilities for converting and processing images (FSLUTILS) tools (FSLROI, FSLSTATS, FSLMATHS). A segmented image and the voxel placement are illustrated in Figure 1B.

Data Analysis

Our molecular neurodevelopmental program, a part of which is reported here, was a combined cross-sectional and longitudinal study with the goal of evaluating subjects across the age range (6–18 years) that covers the physical developmental stages of childhood (6–10 years) pubescence (10–12 years), and adolescence (12–18 years). Subjects were studied at entry and yearly for a total of four assessments. In this report only the cross sectional aspect of the study is considered. Molecular and neuromorphometric findings were obtained from 12 brain regions, 6 in each hemisphere. Values for the targeted metabolites were averaged across the axial slice containing the 12 brain regions thereby yielding a single axial slice value for each metabolite. Our study's primary hypothesis is that neuromolecular underpinnings of synaptic development and elimination, major processes in neurodevelopment, will coincide with or precede changes in percent gray matter and will be observed by differences in the targeted brain metabolites among age groups accompanied by corresponding differences in cognitive function.

To analyze the effect of age and therefore neurodevelopment on the targeted metabolites, scatterplots of age versus average axial slice metabolite levels were obtained and fitted with a locally weighted scatterplot smoothing (LOESS) smoothing function (Cleveland, 1979; Cleveland & Grosse, 1988). The scatterplots (Figure 4) show transition points approximating ages of known neurodevelopment stages, i.e., childhood (6–10 years), pubescence (10–12 years), and adolescence (12–18 years). To more clearly show these transition points for targeted metabolites and percent gray matter, we calculate z values for each (Figure 5). Based on the findings given in Figure 4 and Figure 5, it was elected to compare the 6–9.5 and the 12–18 year old age groups. Comparisons of average metabolite levels between the 6–9.5 and 12–18 years old age groups were performed using two-sided *t* tests.

The same graphic approach was taken in which z-values for PCr, composite cognitive test scores, and percent gray matter were plotted by age (Figure 6). This step was taken so that cognitive function and metabolite levels could be compared with changes in percent cerebral cortical gray matter, which we hypothesized would show an initial growth reflecting synaptic development followed by a reduction because of synaptic elimination.

Next, strength of association between cognitive function and metabolites with age was examined. For this purpose linear multiple regression analyses were performed relating composite scores for the major cognitive domains including language, visual spatial, executive function and memory, to PCr, sPME/sPDE, and NAA levels, as well as percent gray matter. Tests and variables used within each domain are listed in Table 1. Because this is an age-difference study raw scores of cognitive functions were used rather than age corrected standard scores.

RESULTS

MRSI metabolite level changes with age

Average axial slice metabolite levels and percent gray matter were plotted by age using a LOESS smoothing function (Figure 4). These plots demonstrate age-related transition points for PCr, sPME/sPDE, and percent gray matter. The plots show transition points at 9.5 and 12 years. Figure 5 displays the change of PCr, sPME/sPDE ratio, and percent gray matter by converting the metabolite levels and percent gray matter to Z-scores. Guided by these plots and other neurodevelopmental data the metabolite and percent gray matter data were grouped into ages 6–9.5, 9.5–12, and 12–18 years old in order to analyze changes in the metabolite levels with age.

Metabolic Differences Among Age Groups

Descriptive statistics for evaluating differences in PCr, sPME/sPDE, gray matter and composite cognitive scores among the 6–9.5, 9.5–12, and 12–18 years old age groups are presented in Table2. Since there were clear inflections in metabolite levels and percent gray matter in the 6–9.5 and 12–18 year old age groups and a flattening in the 9.5–12 year old group, we performed the statistical analysis as two group comparisons using two-sided *t* tests. The results indicated that comparing 6–9.5 year olds to the 12–18 year olds PCr was lower in the younger age group (PCr, $p = .0001$) and percent gray matter ($p = .0013$) and sPME/sPDE ratio ($p = .046$) were higher. No significant difference was found for NAA comparing the 6–9.5 year olds with 12–18 year olds. The coefficient of variance for PCr (13%) also is much smaller than those for sPME (19%) but similar to those for sPDE (12%) and NAA (9.4%).

Relations Among, PCr Levels, Cognitive Function, and Gray Matter with Age

Of the metabolites measured, PCr is the one which most directly reflects synaptic activity (see Discussion). For purposes of these graphic analyses all scores were converted to z-scores allowing for their comparisons on the same scales. Figure 6 illustrates the profiles of various cognitive domains across the age groups placed on the same graphs as PCr and gray matter percentage. In general, PCr level tracked the cognitive changes quite closely. The rate of PCr increase in the 6–9.5 year olds is similar to the rate of increase in percent gray matter. During the 9.5 to 12 year age range the slope of PCr is approximately flat while percent gray matter sharply decreases. Percentage of gray matter is characterized by an increase in the 6–9.5 year old age group and then a marked decrease in the 9.5–12 year age group with virtually no change from 12 to 18 years. PCr continued to increase in the 12 to 18 year age range.

Correlations of Composite Cognitive scores with MRSI metabolite levels

Multiple linear regression analysis of composite cognitive scores with average axial slice metabolite levels and percent gray matter (Table 3) demonstrated significant correlations of PCr levels with age and language, visual spatial construction, and memory domains. NAA showed a significant correlation only with the visual spatial construction domain. These findings taken together strongly suggest that cognitive function correlates with synaptic activity and not simply the amount of gray matter.

DISCUSSION

In this cross-sectional age difference study we investigated the relationship between a set of ^{31}P-^{1}H MRSI measured metabolites and cognitive development. We did morphological studies for the purpose of evaluating percent gray matter across age groups. The major hypothesis was that neuromolecular underpinnings of synaptic development and elimination would reflect age related cognitive development and coincide or precede change in the percent gray matter.

The hypothesis would be supported if there were significant correlations in the appropriate direction between the metabolites and cognitive tests of varying abilities. We studied tests of language, visual spatial constructional abilities, executive function, and memory. Multiple correlations were computed to evaluate the strength of association between tests within the domains and the metabolites. In general, there was a significant degree of association between changes in the levels of PCr and age-associated improvement in cognitive ability but not with the percent of gray matter.

NAA Levels

NAA (470–974 :moles/100 g) (McIlwain & Bachelard, 1985, pg. 155), which is second to glutamate (781–1250 :moles/100 g) (McIlwain et al., 1985, pg. 155) in terms of total brain concentration of free amino acids, accounts for approximately 85–90% of the proton signal of the N-acetyl methyl group and NAAG contributes to the remaining 10–15% (Koller et al., 1984; Frahm et al., 1991; Pouwels & Frahm, 1997). Both NAA and NAAG are localized exclusively in mature neurons and neuronal processes, and not in mature glia (Tallan et al., 1956; Koller et al., 1984; Birken & Oldendorf, 1989; Urenjak et al., 1993). NAA is formed in mitochondria from acetyl-CoA and aspartate by the membrane bound enzyme L-aspartate N-acetyltransferase, an enzyme found in brain but not in other tissue such as heart, liver and kidney (Goldstein, 1959; Knizley, 1967; Goldstein, 1969; Truckenmiller et al., 1985). Monoclonal antibody studies show NAA to be localized to neurons with intense staining of the perikarya and proximal dendrites axons (Simmons et al., 1991). The neuronal immunoreactivity does not correspond to primary neurotransmitter characteristics. In general, NAA is considered a putative neuronal marker (Arnold et al., 1990) and a recent report of whole brain NAA levels in young adults gave a value of 9.5 ∀ 1.0 mM in white matter an 14.3 ∀ 1.1 mM of gray matter (Inglese et al., 2008). However, in vivo ^{1}H MRS brain studies have shown that decreased NAA is reversible (De Stefano et al., 1995). Therefore, the levels of NAA detected by in vivo ^{1}H MRS also will be dependent on factors that alter the levels of substrates or the activities of the metabolic enzymes as well as tissue factors. Our preliminary studies reveal that the NAA resonance undergoes reversible changes after brief hypoxia (Pettegrew et al., unpublished observations). In addition, factors that change the composition of the tissue sampled such as changing the percent of neurons with long projections or the percent of glial processes will alter NAA levels.

$_{N}$-Acetyl moieties with short correlation times such as found in $_{N}$-acetyl-sugars ($_{N}$-acetyl-galactosamine, $_{N}$-acetyl-glucosamine, $_{N}$-acetyl-neuraminic acid) and glycosphingolipids such as gangliosides also can contribute to the "NAA" resonance. Gangliosides are enriched in gray matter (Agranoff & Hajra, 1994). Evidence indicates that gangliosides are specifically localized in neurons (Lowden & Wolfe, 1964), where gangliosides are enriched in synaptic membranes (Whittaker, 1966; Wiegandt, 1967). The levels of gangliosides in human brain cerebral gray matter (1.45–1.68 mmoles/100 g dry weight) and cerebral white matter (0.28–0.37 mmoles/100 g dry weight) have been determined by Eeg-Olofsson et al. (1966). The levels of gangliosides are developmentally regulated. In the rat brain ganglioside levels start to increase by post-natal day 5 and peak at approximately post-natal day 20 (Suzuki, 1966). Hess et al. (1976) report that human neurons contain 6 times more sialic acid groups than rat brain.

Sialoproteins also contain N-acetylneuraminic acid and could contribute up to 15% of the total brain protein (McIlwain et al., 1985, pg. 316).

sPME/sPDE Ratio

The sPME/sPDE ratio reflects the metabolite turnover of membrane phospholipids such as phosphatidylcholie, phosphatidylethanolamine, and phosphatidylserine. With net synthesis of these phospholipids sPME/sPDE is greater than 1, with net breakdown it is less than 1, and equals 1 when synthesis and breakdown are in equilibrium. Increased sPME are found at the site and time of neuritic sprouting in brain and sPDE are increased at the site and time of membrane breakdown (Geddes et al., 1997). sPME and sPDE are not involved in the synthesis or breakdown of glycosphingolipids such as gangliosides which are enriched in synaptic membranes (Whittaker, 1966; Wiegandt, 1967). sPME/sPDE increases from age 6 to 9.5 years reflecting active synthesis of membrane phospholipids followed by decreases until approximately 14 years of age with evidence for net phospholipid breakdown from age 11 to 14 years. The percent gray matter curve also is shown in Figure 5. As observed, the percent gray matter increases for ages 6 to 9.5 years followed by a steeper decline until approximately 13 years. Changes in percent gray matter were consistent with synaptic development followed by synaptic elimination and are in keeping with the neuromorphometric findings of Giedd et al. (1999) and Gogtay et al. (2007), the molecular findings of Geddes et al. (1997), and the histological data of Huttenlocher and Dabholkar (1997). Note that the rate of increase in percent gray matter from 6–9.5 years and decrease from 9.5 to 13 years is greater than for sPME/sPDE. The difference in these rates (percent gray matter versus sPME/sPDE) could be due to ganglioside contributions to the gray matter.

PCr

Brain contains approximately 3mmole g^{-1} ATP which could maximally provide 6 mmoles g^{-1} of high-energy phosphate. ATP utilization in rat brain is approximately 0.5 mmoles $g^{-1}s^{-1}$ and therefore available stores of ATP would last approximately 12s without new ATP production. However, PCr is a storage form of ATP which can be converted to ATP by the creatine kinase (CrK) enzyme according to the reaction:

$$\mathrm{PCr + ADP + H^+} \underset{\text{E.C.2.7.3.2}}{\overset{\text{CrK}}{\rightleftharpoons}} \mathrm{Cr + ATP}$$

This is an equilibrium reaction ()G = 0), i.e., no net flux in either direction. ATP synthesis is stimulated by a reduction in ATP or increases in ADP or [H^+]. In a comprehensive review Andres et al. (2008) describe PCr as a spatial energy “shuttle” or “circuit” that bridges sites of ATP generation and consumption. Brain concentration of PCr is approximately 5 mmole g^{-1} and therefore the stores of high-energy phosphate (ATP+PCr) will be consumed after about 20s of continuous utilization (Siesjo, 1978, pg. 12). Several studies have shown that anesthesia causes an elevation of PCr and ATP in parallel to the decrease in neuronal activity (McCandless & Wiggins, 1981; Hein et al., 1975). Sokoloff (1991; 1993) also has shown that the synapse is the site of highest energy consumption during increased activity and that most of this consumption is in the recovery period rather than during the activity itself. This is consistent with the studies of Jansson et al. (1979) who showed that PCr and ATP levels are lower in isolated cerebral nerve endings than in whole brain. Unlike nerve tissue in general, synaptosomes preferentially utilize endogenous PCr and ATP stores. Jansson et al. (1979) conclude that synaptic transmission primarily depends on local stores of high-energy phosphates rather than on the availability of glucose per se. Results of human ^{1}H fMRS monitoring of brain PCr levels before, during, and following visual cortical activation are in keeping with the above explanations (Rango et al., 1997; 2001). Other sources of ATP

production such as oxidative phosphorylation and glycolysis come into play after the consumption of PCr pools.

PCr levels are low at age 6 and then sharply increase until age 10. From age 10 to 12 years the increase in PCr levels is much less, but from age 12 to 17 years PCr levels again sharply increase. The low levels of PCr at age 6 years is consistent with the active synthesis of membrane phospholipids which require ATP. For example, one mole of dipalmitoylphosphatidylcholine (DPPC) derived from de novo synthesis requires 295 moles of ATP. Each palmitate requires 145 moles of ATP, uptake of choline requires 1 mole of ATP, synthesis of phosphocholine requires 1 mole of ATP, and the synthesis of the intermediate phosphatidic acid requires 3 moles of ATP. These numbers take into consideration the direct utilization of ATP and the ATP equivalents lost from the utilization of NADH (3 ATP), $FADH_2$ (2 ATP), and acetyl-CoA (12 ATP) in the synthesis of DDPC. The breakdown of DPPC recovers only 258 moles of ATP from the oxidation of both palmitates. Therefore, the complete synthesis and breakdown of 1 mole of DPPC results in an energetic debt of 37 moles of ATP. The acylation/deacylation of DPPC results in an energetic debt of 2 moles of ATP. Likewise, the de novo synthesis of 1 mole of cholesterol, a major membrane constituent requires 276 moles of ATP with no ATP recovered from the breakdown of cholesterol (Pettegrew et al., 2003).

The slow increase in PCr levels from ages 9.5–12 years coincides with a steep decrease in gray matter volume and less rapid decrease in the sPME/sPDE ratio. One might speculate that the membranes being lost are predominantly non-phosphorus containing glycosphingolipids such as gangliosides which are predominantly found in gray matter and are enriched in synaptic membranes. By this reasoning, the decrease in gray matter is most likely due to decrease in synaptic membranes contained in the neuropil.

The decline in gray matter volume from 12–18 years corresponds to continued increases in PCr. In the brain ATP is primarily consumed at synaptic membranes for repolarizing synaptic membranes which have been depolarized and PCr is the buffer for ATP (Buchli et al., 1994; Chugani et al., 1987; Frey, 1994; Hein et al., 1975; Hess, 1961; Jansson et al., 1979; Kadekaro et al., 1985; Kennedy & Sokoloff, 1957; McCandless et al., 1981; Sokoloff, 1966; 1991). The increase in PCr in the 12–18 year olds could be caused by synaptic elimination resulting in fewer synapses or decreased activity of remaining synapses in older subjects.

Correlations Among PCr Levels, Gray Matter Volume, and Cognitive Composite Scores

Both PCr and percent gray matter in the axial slice are highly correlated with age, but NAA, sPME, sPDE, and sPME/sPDE are not. In addition, both PCr and percent gray matter in the axial slice are correlated with language, visual spatial construction, and memory but not with executive function. Finally, PCr levels and percent gray matter in the axial slice correlate ($r = -.304$, $p = .0026$) with each other, but NAA and percent gray matter are not correlated ($r = -.023$; $p = .835$). These findings taken together and inspection of Figure 6 suggests that axial slice PCr levels in general follow a curve similar to curves for the various cognitive domains. However, the curve for percent gray matter has qualitative findings dissimilar to the curve for PCr which is consistent with synaptic elimination (percent gray matter curve) and the functional consequence of synaptic elimination or reduced synaptic activity (PCr curve). Finally, given the lack of correlation between NAA and percent gray matter, it may be there are other molecular contributions to the "NAA" resonance signal besides N-acetylaspartate as discussed above. Regional analyses of these data is in progress and will be extremely useful to address some of these issues, such as whether synaptic elimination in PFC is occurring later than regions such as STC or IPC.

Conclusions

These conclusions are based on cross-sectional analysis and there would be clear advantages to testing our subjects longitudinally. We have done so, and will report the findings in a future publication. We would note though that it is not likely that the cross-sectional data were markedly influenced by cohort effects since all subjects were recruited from the same community over a period of only four years. There is the possibility of gender differences which we could not evaluate here because of small sample sizes. A final consideration is that the study was limited to an axial slice of brain measures of PCr, sPME, sPDE, and NAA and different results may be found at different regional locations. Since we had the capability of obtaining MRS measures from various brain regions, we will present the findings in a future report.

Acknowledgments

This work was supported in part by an NIHCD/NIH HD-39799 grant (JWP). We thank Terry Bradbury for conducting neuropsychological testing. Indebtedness is also expressed to the Medical Research Service and the VISNIV Mental Illness, Research, Education and Clinical Center (MIRECC), Department of Veterans Affairs for support of this work. We thank Harriet Marshman, Deborah Wetzler and Dennis McKeag for help in conducting the study.

REFERENCES

Agranoff, BW.; Hajra, AK. Lipids. In: Siegel, GJ.; Agranoff, BW.; Albers, RW.; Molinoff, PB., editors. Basic Neurochemistry, Molecular, Cellular, and Medical Aspects. Vol. 5th ed. New York: Raven Press; 1994. p. 97-116.

Andreasen NC, Endicott J, Spitzer RL, Winoker G. The reliability and validity of the family history method using family history research diagnostic criteria (FH-RDC). Archives of General Psychiatry 1977;34:1229–1235. [PubMed: 911222]

Andres RH, Ducray AD, Schlattner U, Wallimann T, Widmer HR. Functions and effects of creatine in the central nervous system. Brain Research Bulletin 2008;76:329–343. [PubMed: 18502307]

Arnold DL, Matthews PM, Francis G, Antel J. Proton magnetic resonance spectroscopy of human brain in vivo in the evaluation of multiple sclerosis: Assessment of the load of disease. Magnetic Resonance in Medicine 1990;14:154–159. [PubMed: 2161982]

Bartha R, Drost DJ, Menon RS, Williamson PC. Comparison of the quantification precision of human short echo time (1)H spectroscopy at 1.5 and 4.0 Tesla. Magnetic Resonance in Medicine 2000;44:185–192. [PubMed: 10918316]

Birch, HG.; Gussow, JD. Disadvantaged children, health, and nutrition and school failure. New York: Harcourt, Brace & World; 1970.

Birken DL, Oldendorf WH. N-Acetyl-L-aspartic acid: A literature review of a compound prominent in ^{1}H-NMR spectroscopic studies of brain. Neuroscience and Biobehavioral Reviews 1989;13:23–31. [PubMed: 2671831]

Bottomley PA. Spatial localization in NMR spectroscopy in vivo. Annals of the New York Academy of Sciences 1987;508:333–348. [PubMed: 3326459]

Bourgeois J-P, Rakic P. Changes of synaptic density in the primary visual cortex of the Macaque monkey from fetal to adult stage. Journal of Neuroscience 1993;13:2801–2820. [PubMed: 8331373]

Brockmann K, Pouwels PJ, Christen HJ, Frahm J, Hanefeld F. Localized proton magnetic resonance spectroscopy of cerebral metabolic disturbances in children with neuronal ceroid lipofuscinosis. Neuropediatrics 1996;27:242–248. [PubMed: 8971744]

Buchli R, Martin E, Boesiger P, Rumpel H. Developmental changes of phosphorus metabolite concentrations in the human brain: A ^{31}P magnetic resonance spectroscopy study *in vivo*. Pediatric Research 1994;35:431–435. [PubMed: 8047379]

Chugani HR, Phelps ME, Mazziotta JC. Positron emission tomography study of human brain functional development. Annals of Neurology 1987;322:487–497. [PubMed: 3501693]

Cleveland WS. Robust locally-weighted regression and smoothing scatterplots. Journal of the American Statistical Association 1979;74:829–836.

Cleveland WS, Grosse E. Regression by local fitting. Journal of Econometrics 1988;37:87–114.

de Beer, R.; van Ormondt, D. Analysis of NMR data using time domain fitting procedures. In: Diehl, P.; Fluck, EG., editors. NMR Basics, Principles and Progress. New York: Springer-Verlag; 1992. p. 201-258.

De Stefano N, Matthews PM, Arnold DL. Reversible decreases in N-acetylaspartate after acute brain injury. Magnetic Resonance in Medicine 1995;34:721–727. [PubMed: 8544693]

deGraaf AA, Bovee WMMJ. Improved quantification of *in vivo* ^{1}H NMR spectra by optimization of signal acquisition and processing and by incorporation of prior knowledge into the spectral fitting. Magnetic Resonance in Medicine 1990;15:305–319. [PubMed: 1975420]

Ebert D, Speck O, Konig A, Berger M, Hennig J, Hohagen F. 1H-magnetic resonance spectroscopy in obsessive-compulsive disorder: evidence for neuronal loss in the cingulate gyrus and the right striatum. Psychiatry Research 1997;74:173–176. [PubMed: 9255862]

Eeg-Olofsson O, Kristensson K, Sourander P, Svennerholm L. Tay-Sach's Disease. A generalized emtabolic disorder. Acta Paediatrica Scandinavia 1966;55:546–562.

Frahm J, Hanefeld F. Localized proton magnetic resonance spectroscopy of cerebral metabolites. Neuropediatrics 1996;27:64–69. [PubMed: 8737820]

Frahm J, Michaelis T, Merboldt KD, Hanicke W, Gyngell ML, Bruhn H. On the N-acetyl methyl resonance in localized ^{1}H NMR spectra of human brain *in vivo*. Nuclear Magnetic Resonance in Biomedicine 1991;4:201–204.

Frey, KA. Positron emission tomography. In: Siegel, GJ.; Agranoff, BW.; Albers, RW.; Molinoff, PB., editors. Basic Neurochemistry: Molecular, Cellular and Medical Aspects. Vol. 5 ed. New York: Raven Press; 1994. p. 935-955.

Geddes JW, Panchalingam K, Keller JN, Pettegrew JW. Elevated phosphocholine and phosphatidyl choline following rat entorhinal cortex lesions. Neurobiology of Aging 1997;18:305–308. [PubMed: 9263196]

Giedd JN, Blumenthal J, Jeffries NO, Castellanos FX, Liu H, Zijdenbos A, Paus T, Evans AC, Rapoport JL. Brain development during childhood and adolescence: a longitudinal MRI study. Nature Neuroscience 1999;2:861–863.

Gogtay N, Ordonez A, Herman DH, Hayashi KM, Greenstein D, Vaituzis C, Lenane M, Clasen L, Sharp W, Giedd JN, Jung D, Nugent TF III, Toga AW, Leibenluft E, Thompson PM, Rapoport JL. Dynamic mapping of cortical development before and after the onset of pediatric bipolar illness. Journal of Child Psychology & Psychiatry & Allied Disciplines 2007;48:852–862.

Goldstein FB. Biosynthesis of N-acetyl-L-aspartic acid. Journal of Biological Chemistry 1959;234:2702–2706.

Goldstein FB. The enzymatic synthesis of N-acetyl-L-aspartic acid by subcellular preparations. Journal of Biological Chemistry 1969;244:4257–4260. [PubMed: 5800445]

Hein H, Krieglstein J, Stock R. The effects of increased glucose supply and thiopental anesthesia on energy metabolism of the isolated perfused rat brain. Naunyn Schmiedebergs Archives of Pharmacology 1975;289:399–407.

Hess, H. The rates of respiration of neurons and neuroglia in human cerebrum. In: Kety, SS.; Elkes, J., editors. Regional Neurochemistry. Oxford: Pergamon Press; 1961. p. 200-202.

Hess HH, Bass NH, Thalheimer C, Devarakonda R. Gangliosides and the architecture of human frontal and rat somatosensory isocortex. Journal of Neurochemistry 1976;26:1115–1121. [PubMed: 932717]

Huttenlocher PR. Synaptic density in human frontal cortex. Developmental changes and effects of aging. Brain Research 1979;163:195–205. [PubMed: 427544]

Huttenlocher PR. Morphometric study of human cerebral cortex development. Neuropsychologia 1990;28:517–527. [PubMed: 2203993]

Huttenlocher PR, Dabholkar AS. Regional differences in synaptogenesis in human cerebral cortex. Journal of Comparative Neurology 1997;387:167–178. [PubMed: 9336221]

Huttenlocher PR, de Courtten C, Garey LJ, Van der Loos LH. Synaptogenesis in human visual cortex--evidence for synapse elimination during normal development. Neuroscience Letters 1982;33:247–252. [PubMed: 7162689]

Inglese M, Rusinek H, George IC, Babb JS, Grossman RI, Gonen O. Global average gray and white matter N-acetylaspartate concentration in the human brain. Neuroimage 2008;41:270–276. [PubMed: 18400521]

Jansson SE, Harkonen MH, Helve H. Metabolic properties of nerve endings isolated from rat brain. Acta Physiologica Scandinavica 1979;107:205–212. [PubMed: 539452]

Kadekaro M, Crane AM, Sokoloff L. Differential effects of electrical stimulation of sciatic nerve on metabolic activity in spinal cord and dorsal root ganglion in the rat. Proceedings of the National Academy of Sciences of the United States of America 1985;82:6010–6013. [PubMed: 3862113]

Kennedy C, Sokoloff L. An adaptation of the nitrous oxide method to the study of the cerebral circulation in children; normal values for cerebral blood flow and cerebral metabolic rate in childhood. Journal of Clinical Investigation 1957;36:1130–1137. [PubMed: 13449166]

Klunk WE, Xu CJ, Panchalingam K, McClure RJ, Pettegrew JW. Analysis of magnetic resonance spectra by mole percent: Comparison to absolute units. Neurobiology of Aging 1994;15:133–140. [PubMed: 8159259]

Knizley H. The enzymatic synthesis of N-acetyl-L-aspartic acid by a water-insoluble preparation of a cat brain acetone powder. Journal of Biological Chemistry 1967;242:4619–4622. [PubMed: 6061408]

Koller KJ, Zaczek R, Coyle J. N-acetyl-aspartyl-glutamate: Regional levels in rat brain and the effects of brain lesions as determined by a new HPLC method. Journal of Neurochemistry 1984;43:1136–1142. [PubMed: 6470709]

Kreis R. Quantitative localized ^{1}H MR spectroscopy for clinical use. Journal Progress Nuclear Magnetic Resonance 1997;31:155–195.

Lowden JA, Wolfe LS. Studies on brain gangliosides. III Evidence for the location of gangliosides specifically in neurones. Canadian Journal of Biochemistry 1964;42:1587–1594.

McCandless DW, Wiggins RC. Cerebral energy metabolism during the onset and recovery from halothane anesthesia. Neurochemical Research 1981;6:1319–1326. [PubMed: 7339509]

McIlwain, H.; Bachelard, HS. Biochemistry and the Central Nervous System. Vol. 5 ed. Edinburgh: Churchill Livingstone; 1985.

Pettegrew, JW.; Keshavan, MS.; Stanley, JA.; McClure, RJ.; Johnson, CR.; Panchalingam, K. Magnetic resonance spectroscopy in the assessment of phospholipid metabolism in schizophrenia and other psychiatric disorders. In: Peet, M.; Glen, I.; Horrobin, DF., editors. Phospholipid Spectrum Disorder in Psychiatry. Vol. 2nd ed. Carnforth, UK: Marius; 2003. p. 239-255.

Pouwels PJ, Frahm J. Differential distribution of NAA and NAAG in human brain as determined by quantitative localized proton MRS. Nuclear Magnetic Resonance in Biomedicine 1997;10:73–78.

Provencher SW. Estimation of metabolite concentrations from localized *in vivo* proton NMR spectra. Magnetic Resonance in Medicine 1993;30:672–679. [PubMed: 8139448]

Rakic P, Bourgeois J-P, Eckenhoff MF, Zecevic N, Goldman-Rakic PS. Concurrent overproduction of synapses in diverse regions of the primate cerebral cortex. Science 1986;232:232–235. [PubMed: 3952506]

Rango M, Bozzali M, Prelle A, Scarlato G, Bresolin N. Brain activation in normal subjects and in patients affected by mitochondrial disease without clinical central nervous system involvement: a phosphorus magnetic resonance spectroscopy study. Journal of Cerebral Blood Flow & Metabolism 2001;21:85–91. [PubMed: 11149672]

Rango M, Castelli A, Scarlato G. Energetics of 3.5 s neural activation in humans: a ^{31}P MR spectroscopy study. Magnetic Resonance in Medicine 1997;38:878–883. [PubMed: 9402187]

Roux L. Magnetic Resonance. Journal of Magnetic Resonance Imaging 1998;8:1022–1023. [PubMed: 9786138]

Seeger U, Klose U, Mader I, Grodd W, Nagele T. Parameterized evaluation of macromolecules and lipids in proton MR spectroscopy of brain diseases. Magnetic Resonance in Medicine 2003;49:19–28. [PubMed: 12509816]

Siesjo, BK. Brain Energy Metabolism. New York: John Wiley & Sons; 1978.

Simmons ML, Frondoza CG, Coyle JT. Immunocytochemical localization of N-acetyl-aspartate with monoclonal antibodies. Neuroscience 1991;45:37–45. [PubMed: 1754068]

Smiley JF, Goldman-Rakic PS. Heterogeneous targets of dopamine synapses in monkey prefrontal cortex demonstrated by serial section electron microscopy: A laminar analysis using the silver enhanced

diaminobenzidine-sulfide (SEDS) immunolabeling technique. Cerebral Cortex 1993;3:223–238. [PubMed: 7686795]

Smith SM, Jenkinson M, Woolrich MW, Beckmann CF, Behrens TEJ, Johansen-Berg H, Bannister PR, De Luca M, Drobnjak I, Flitney DE, Niazy R, Saunders J, Vickers J, Zhang Y, De Stefano N, Brady JM, Matthews PM. Advances in functional and structural MR image analysis and implementation as FSL. Neuroimage 2004;23(S1):208–219.

Sokoloff L. Cerebral circulatory and metabolic changes associated with aging. Research Publications - Association for Research in Nervous and Mental Disease 1966;41:237–254. [PubMed: 5957649]

Sokoloff L. Measurement of local cerebral glucose utilization and its relation to local functional activity in the brain. Advances In Experimental Medicine & Biology 1991;291:21–42. [PubMed: 1927683]

Sokoloff L. Function-related changes in energy metabolism in the nervous system: localization and mechanisms. Keio Journal of Medicine 1993;42:95–103. [PubMed: 8255068]

Stanley JA, Drost DJ, Williamson PC, Thompson RT. The use of *a priori* knowledge to quantify short echo *in vivo* ^{1}H MR spectra. Magnetic Resonance in Medicine 1995;34:17–24. [PubMed: 7674893]

Stanley JA, Pettegrew JW. Post-processing method to segregate and quantify the broad components underlying the phosphodiester spectral region of *in vivo* 31-P brain spectra. Magnetic Resonance in Medicine 2001;45:390–396. [PubMed: 11241695]

Storm-Mathisen J, Otterson OP. Immunocytochemistry of glutamate at the synaptic level. Journal of Histochemistry and Cytochemistry 1990;38:1733–1743. [PubMed: 1979340]

Suzuki K. The pattern of mammalian brain gangliosides III. Regional and developmental differences. Journal of Neurochemistry 1966;12:969–979.

Tallan HH, Moore S, Stein WH. N-acetyl-L-aspartic acid in brain. Journal of Biological Chemistry 1956;219:257–264. [PubMed: 13295277]

Truckenmiller ME, Namboodiri MAA, Brownstein MJ, Neale JH. N-Acetylation of L-aspartate in the nervous system: Differential distribution of a specific enzyme. Journal of Neurochemistry 1985;45:1658–1662. [PubMed: 4045470]

Urenjak J, Williams SR, Gadian DG, Noble M. Proton nuclear magnetic resonance spectroscopy unambiguously identifies different neural cell types. Journal of Neuroscience 1993;13:981–989. [PubMed: 8441018]

Whittaker VP. Some properties of synaptic membranes isolated from the central nervous system. Annals of the New York Academy of Sciences 1966;137:982–998. [PubMed: 5229839]

Wiegandt H. The subcellular localization of gangliosides in the brain. Journal of Neurochemistry 1967;14:671–674. [PubMed: 6025100]

Woolrich MW, Jbabdi S, Patenaude B, Chappell M, Makni S, Behrens T, Beckmann C, Jenkinson M, Smith SM. Bayesian analysis of neuroimaging data in FSL. Neuroimage 2009;45:S173–S186. [PubMed: 19059349]

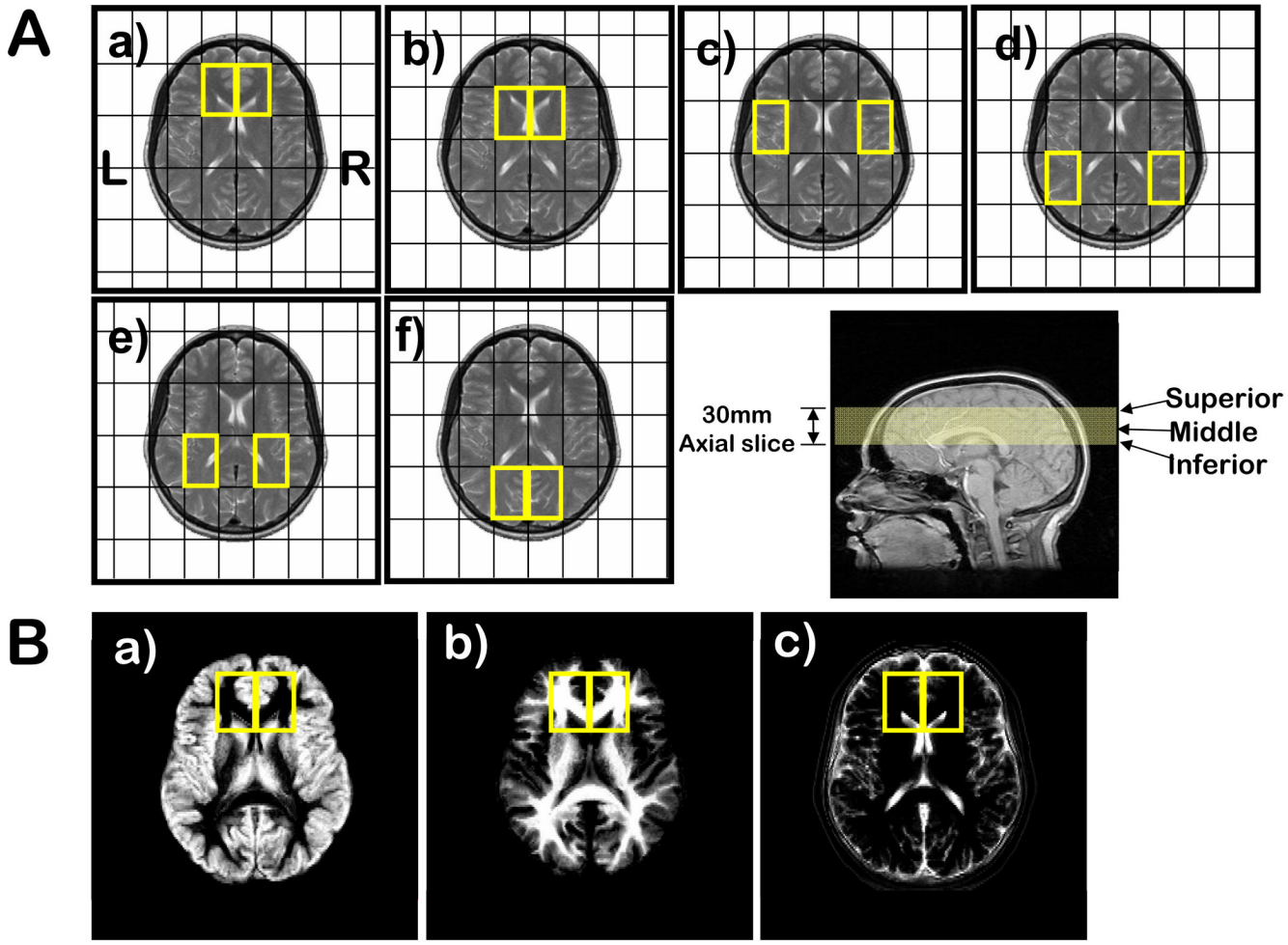

Figure 1.

(A) ^{31}P MRSI voxel grid shifts (outlined in yellow) superimposed on the middle MRI axial slice (bottom right) for: **a)** prefrontal cortex; **b)** basil ganglia; **c)** superior temporal cortex; **d)** inferior parietal cortex; **e)** centrum semiovale; and **f)** occipital regions. Voxel size is 45×45×30 mm^3. **(B)** Segmentation images of: **a)** gray matter; **b)** white matter; and **c)** CSF and extra-cortical matter where the intensity is proportional to the tissue type of that image. The matrix size of the images is 256 in the sagittal direction by 124 in the coronal direction, reflecting the 124 slices that were acquired for the 3-dimensional SPGR sequence. Right and left ^{31}P prefrontal voxels (yellow boxes) are superimposed on the images.

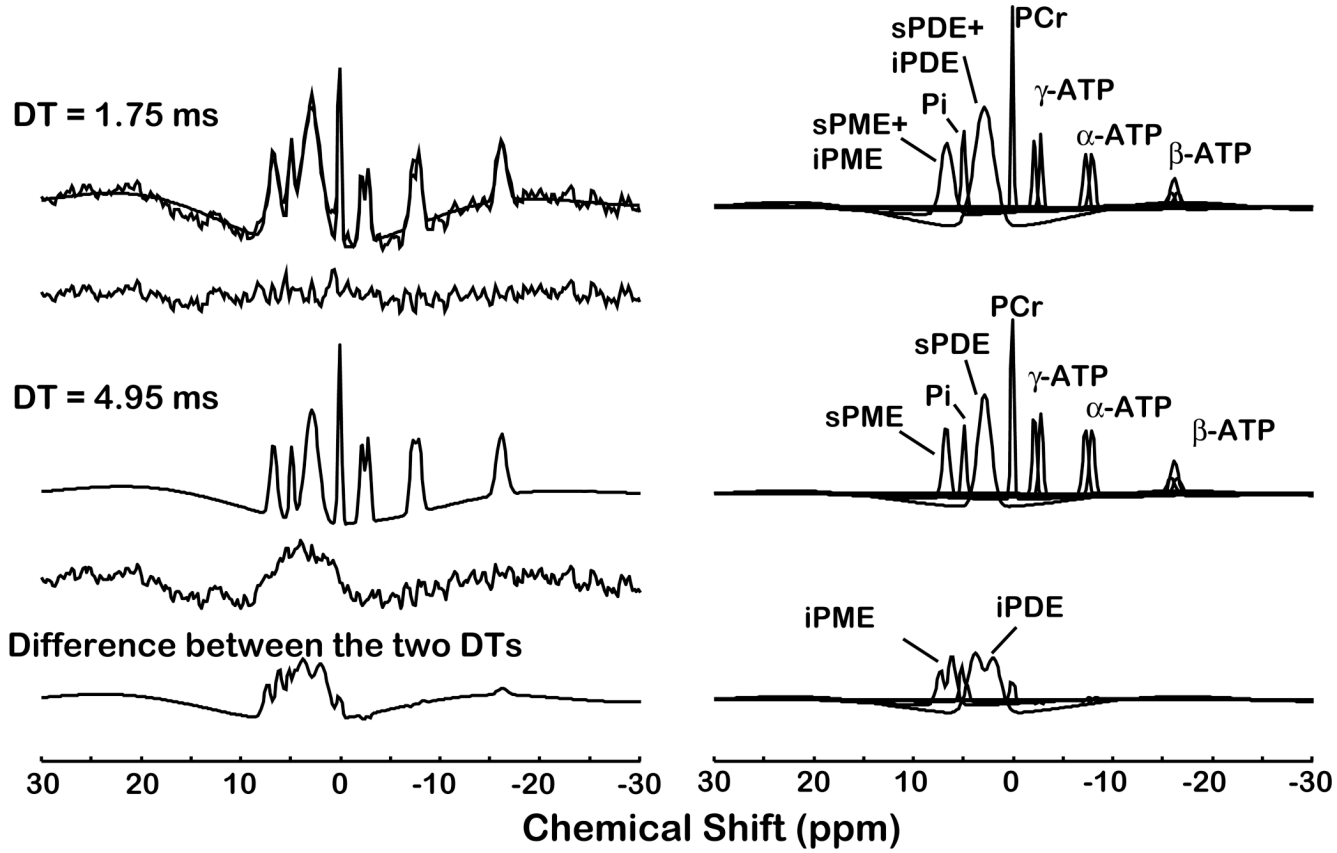

Figure 2.

Quantification of a typical in vivo ^{31}P magnetic resonance spectroscopic imaging spectrum with 5 Hz line broadening from a single voxel (30×30×30 mm^3) of a study subject. The acquired spectrum is modeled in the time domain with Gaussian-damped sinusoids and by omitting both the first 0.75 ms and first 2.75 ms of the free induction decay using the Marquardt-Levenberg algorithm. Both the short (0.75 ms) and long (2.75 ms) delay time (DT) models are shown superimposed on the acquired ^{31}P spectra and the modeled resonances are identified on the right. The difference between the two time domain fits results in the bottom trace containing the intermediate correlation time components.

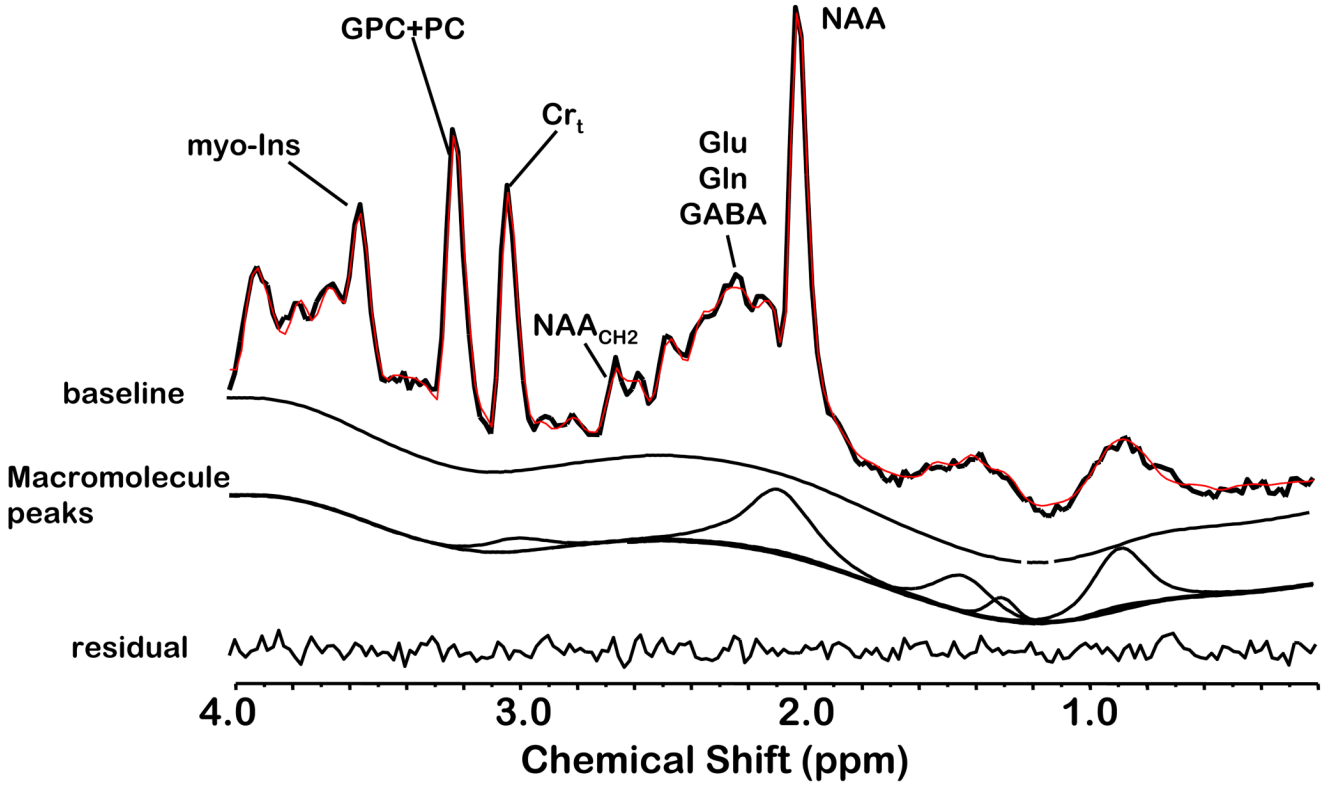

Figure 3.
An example of quantifying a short TE ^{1}H MRSI spectrum of a control subject using the proposed acquisition protocol and LC Model fitting. The acquired spectrum with no line broadening is superimposed on the modeled and baseline spine function and the residual is below. The quantified macromolecule signal is indicated in a separate trace.

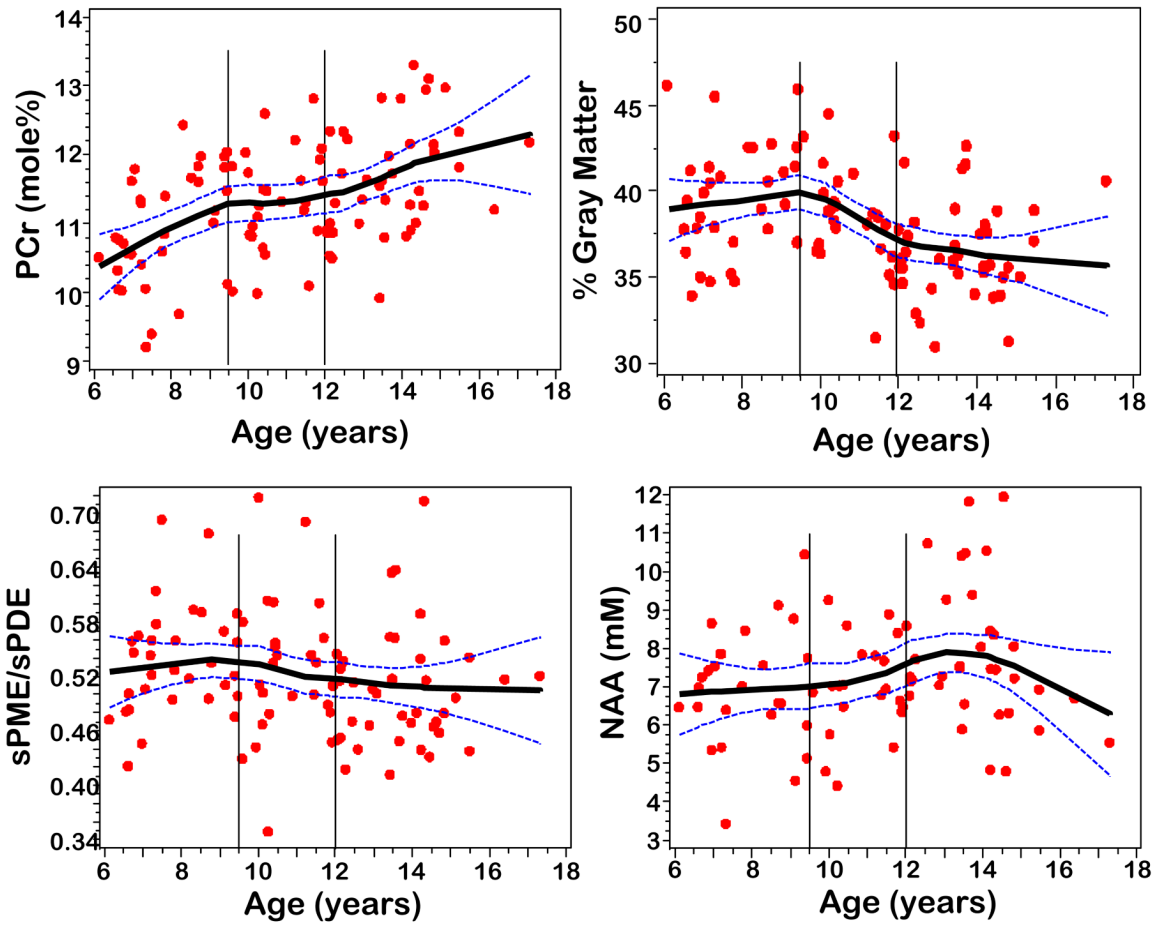

Figure 4A

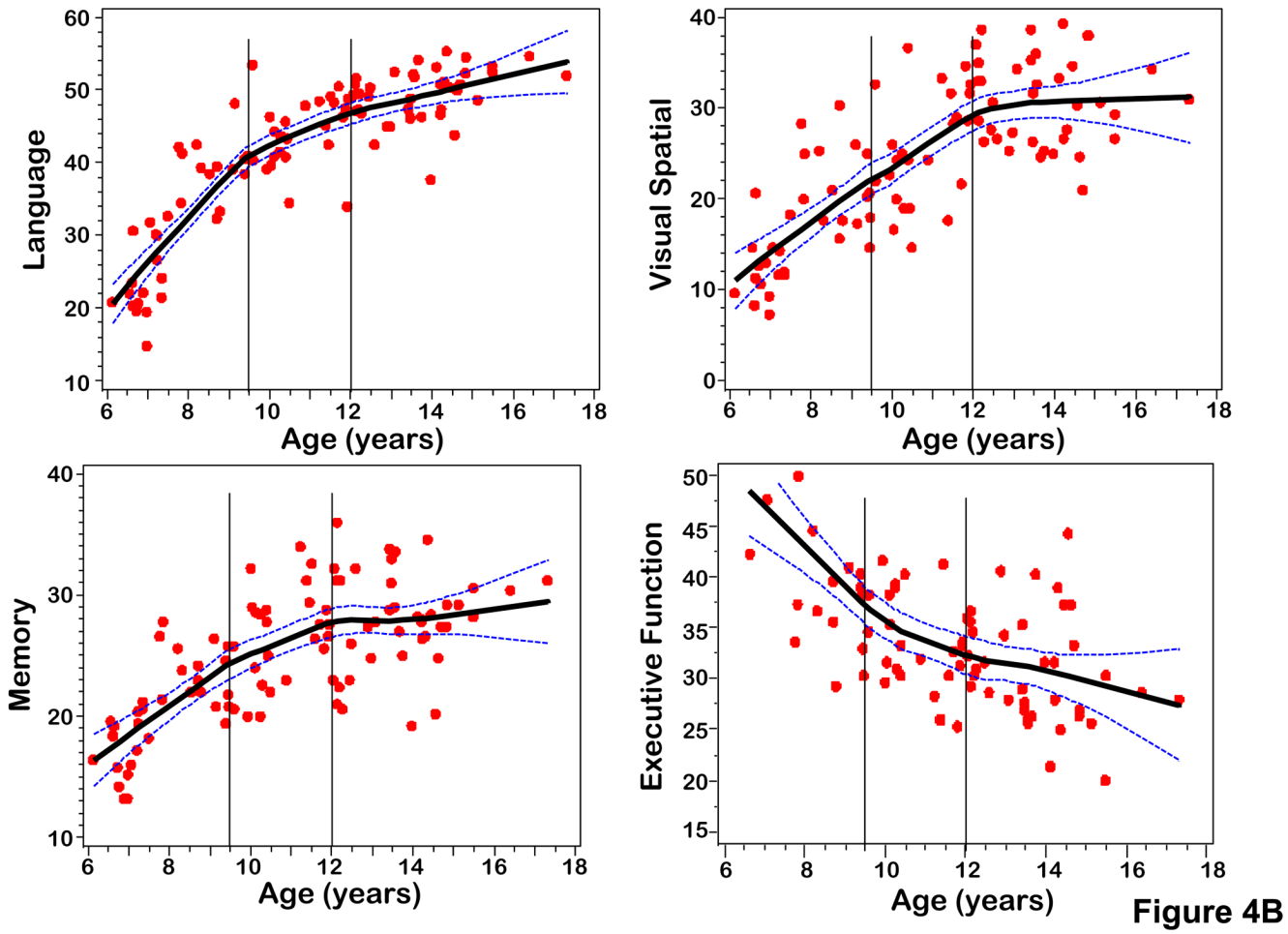

Figure 4.

(A) Scatterplots of PCr, sPME/sPDE, NAA, gray matter volume versus age fitted with a LOESS curve with 95% confidence intervals. **(B)** Scatterplots of composite scores for cognitive domains (Language, Memory, Visual Spatial, Executive Function) versus age fitted with a LOESS curve with 95% confidence intervals.

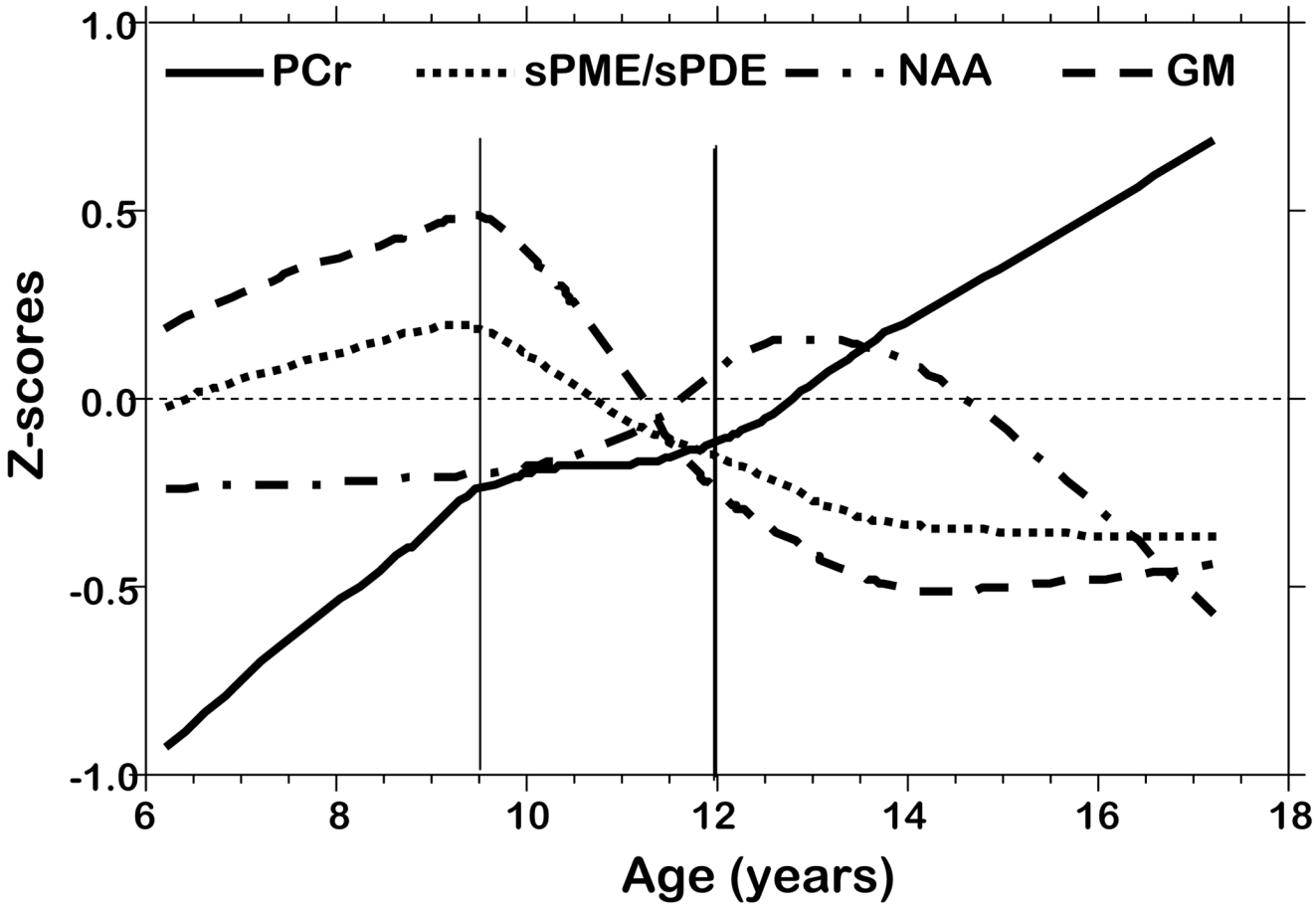

Figure 5.
Z-score plots of PCr, sPME/sPDE, NAA, and gray matter volume versus age.

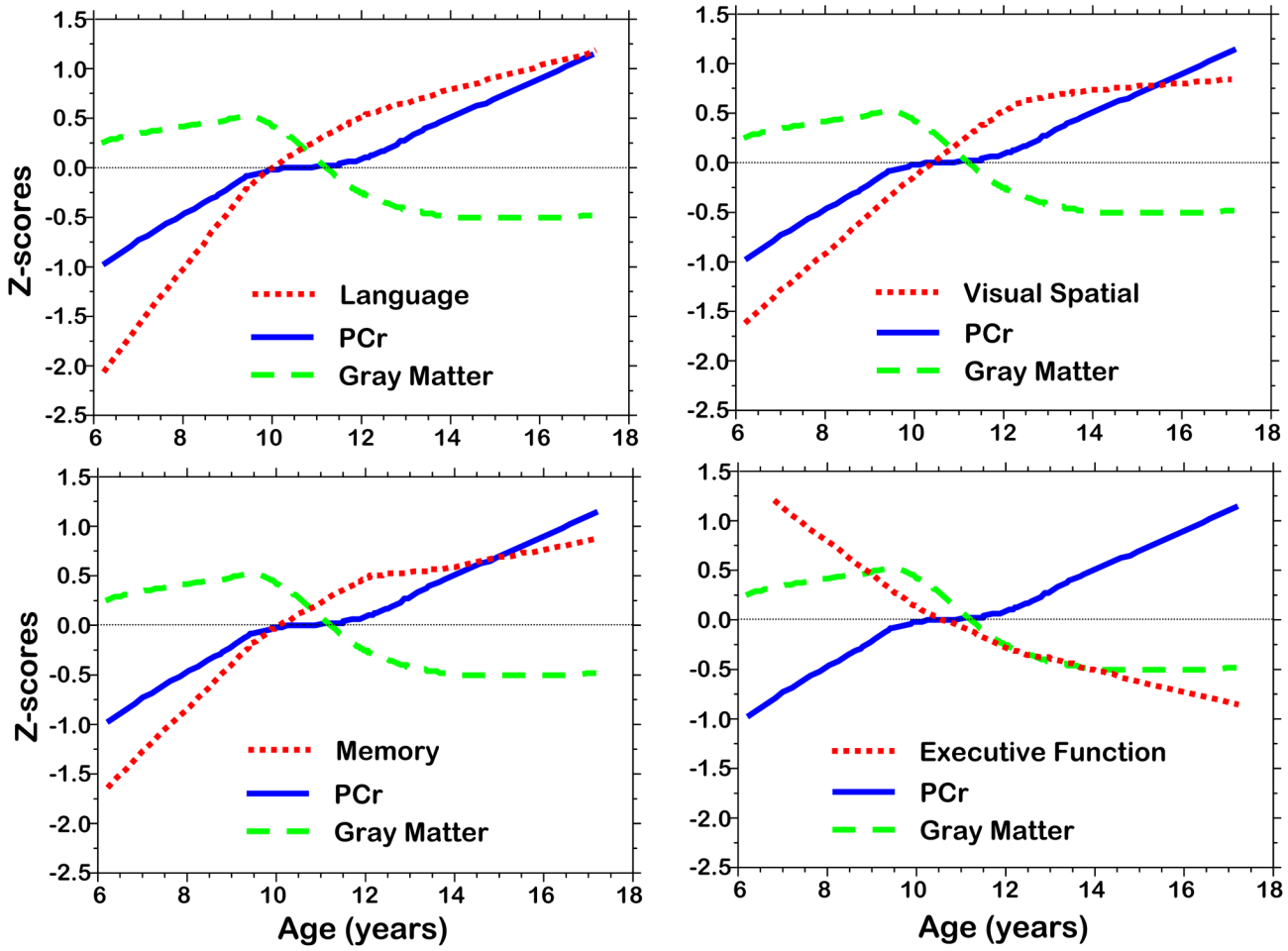

Figure 6.
Z-score plots of PCr, gray matter volume, cognitive domain composite scores (Language, Memory, Visual Spatial, Executive Function).

Table 1

Neuropsychological test variables used within each cognitive domain.

DOMAIN	TEST	VARIABLES
Language	Abbreviated WISC for children	Total Verbal raw scores
	Wechsler Individual Scale of Intelligence (WASI) for Adults	Total Verbal raw scores
	Wechsler Individual Achievement Test (WIAT)	Reading, Spelling raw scores
	Clinical Evaluation of Language Fundamentals (CELF)	Concepts and Directions raw scores
	Peabody Picture Vocabulary Tests	Raw scores
Executive Function	Wechsler Similarities and Matrix Reasoning Subtests	Raw scores
	Wisconsin Card Sorting Test	Perseverative Errors
Visual Spatial	Wechsler Block Design	Raw score
	Visual Motor Integration Test	Raw score
	Test of Visual Perception	Spatial Relations Subtest- raw score
Memory	Wide Range Assessment of Memory and Learning (WRAML)	Picture Memory, Design Memory, Verbal Learning, Story Memory and Number/Letter Subtests

Table 2

Descriptive statistics of axial slice MRSI metabolites and percent gray matter by age group.

Age Group	**6 – 9.5 (years)**		**9.5 – 12 (years)**		**12 – 18 (years)**		**6 – 9.5 vs. 12–18**
	***M* ± SD**	**N**	***M* ± SD**	**N**	***M* ± *SD***	***N***	***p*-value**
sPME/sPDE (ratio mole %)	0.538 ± 0.059	33	0.528 ± 0.78	26	0.507 ± 0.063	40	.046
PCr (mole %)	10.95 ± 0.82	33	11.33 ± 0.74	26	11.66 ± 0.81	40	.0001
NAA (mM)	6.98 ± 1.52	26	6.98 ± 1.26	21	7.82 ± 1.82	35	Not Significant
Gray Matter(% volume)	39.88 ± 3.45	26	38.65 ± 2.90	25	36.31 ± 2.94	40	.0013

Table 3

Multiple linear regression analysis relating composite scores for cognitive domains with MRSI metabolite levels and percent gray matter.

	Age		Language		Visual Spatial		Executive Function		Memory	
	r	N	r	N	r	N	r	N	r	N
PCr	.474***	99	.421***	96	.234*	94	.076	79	.291**	98
sPME/sPDE	−.150	98	−.064	95	−.108	94	.008	79	.009	97
NAA	.208	85	.173	83	.237*	81	.135	69	.159	85
Gray Matter	−.399***	81	−.287*	78	−.368***	76	−.223	69	−.323**	80